Available online at www.sciencedirect.com
ScienceDirect
Trans. Nonferrous Met. Soc. China 27(2017) 591−598
Transactions of Nonferrous Metals Society of China
www.tnmsc.cn

Red mud and fly ash-based ceramic foams using starch and manganese dioxide as foaming agent

Li-jun HOU, Tao-yong LIU, An-xian LU

School of Materials Science and Engineering, Central South University, Changsha 410083, China

Received 21 January 2016; accepted 21 September 2016

Abstract: Ceramic foams were prepared using red mud and fly ash as raw materials with sodium borate as sintering aid agent, starch and MnO_2 as foaming agent, respectively. The influence of the amount of starch or MnO_2 on the crystalline phase, pore morphology and physical–chemical porosities was studied. The results showed that the main crystal phases of samples with starch addition and MnO_2 addition were sodalite phase $Na_6(AlSiO_4)_6$ and $Na_8(SiAlO_4)_6MnO_4$, respectively. The SEM images showed that the variation of porous structure was mainly dominated by the addition of foaming agent. With the increase of foaming agent, the samples exhibited better comprehensive properties: bulk density of 0.59−0.96 g/cm^3, porosity of 41.82%−63.51%, water absorption of 3.16%−9.17%, compressive strength of 4.22−8.38 MPa, flexural strength of 2.44−5.82 MPa, acid resistance of 95.59%−99.60%, alkali resistance of 99.82%−99.99%. Based on these properties, the ceramic foams can be used in building field.

Key words: red mud; fly ash; starch; manganese dioxide; ceramic foam

1 Introduction

Industrial solid waste pollution from the metallurgical industries has become an increasingly serious problem all over the world. Every year, large quantities of metallurgical wastes are generated from the production of various metals. In these solid wastes, red mud from alkali leaching [1] of bauxite by the Bayer process for producing aluminum oxide (Al_2O_3) [2] and fly ash generated through coal-based thermal power plants have been heavily accumulated and continuously increased [3] for a long time. These residues are considered as hazardous wastes due to their soluble metal content which induces many social problems such as contaminated water [4,5], dust-laden air [6,7] and alkalized soils [8,9], as well as human and animal health [10,11] and security risks from the collapse of wastes. In China, fly ash is generally stored at coal-fired power plants or placed in landfills. About 40% of fly ash is recycled, which was used to supplement Portland cement [12] in concrete production. As for red mud, filling and stacking are yet two major means of its maximizing utilization until recently [13,14].

In recent years, intensive research and development efforts have been directed towards finding compatible solutions for red mud minimization and utilization [15], including decreasing quantities of emissions, maximizing levels of utilization and developing of high value products. Many new kinds of materials have been developed by using red mud as major raw materials, such as soil amendment for pollutants in liquid and solid phases [16], water treatment [17,18], metal recovery (Fe, Al and Ti) [19], radio-opaque materials [20], glass-ceramics [21] and ceramics [22]. The authors believe that the preparation and application of building ceramic foams may be an effective solution for the minimization of wastes and utilization of high value. On one hand, construction industry has an enormous market need for building ceramic foams. Mass production of ceramic foams will obviously decrease the total of wastes which can be used as raw materials, resulting in the alleviation of environmental problems. On the other hand, ceramic foams are high value products with multi-functions such as thermal insulation, acoustic insulation, fire-proof, and freezing tolerance. The wide applications of ceramic foams would lead to a significant reduction of energy consumption and fire disaster in buildings. In our previous studies, foam glasses containing 70% of fly ash [23,24] and ceramic foams with 80% of red mud

Foundation item: Project (K1003027-11) supported by the Key Project Foundation of Science and Technology Plans of Changsha, China
Corresponding author: An-xian LU; Tel: +86-731-88830351; Fax: +86-731-88877057; E-mail: axlu@csu.edu.cn
DOI: 10.1016/S1003-6326(17)60066-9

and fly ash [25] have been prepared by using sodium silicate solution (commonly known as water glass) with 2:1 of SiO_2:Na_2O molar ratio as foaming agent. According to Ref. [25], sodium silicate could be used as an excellent forming agent in the production of porous materials. As a viscous foaming agent, however, there are some problems existing in its application such as inconvenient weighing and difficult to guarantee the uniformity of batch mixing. Thus, the dry solid particle foaming agent was chosen for avoiding the inconvenient of weighing raw materials and guaranteeing the uniformity of batch mixing. Generally, starch and MnO_2 are used as common foaming agent to prepare porous materials in Res. [26−28]. However, few reports have been discussed on the preparation of ceramic foams combining fly ash and red mud as raw materials with starch and MnO_2 as foaming agent.

In this work, red mud and fly ash based ceramic foams were investigated by using starch and MnO_2 as foaming agents respectively, and sodium borate as sintering aid agent. The effects of foaming agent content on the crystalline phase, microstructure, physical–mechanical porosities and chemical stability of glass ceramic foams were investigated.

2 Experimental

2.1 Raw materials

The starting materials used in this work were red mud, fly ash and analytically pure sodium borate $Na_2B_4O_7$ (99%), as well as soluble starch $(C_6H_{10}O_5)_n$ (99.5%) and MnO_2 (97.85%). Fly ash and red mud used in the present experiments were supplied by Leiyang Power Plant and Henan Aluminum Co., Ltd, respectively. The pure sodium borate and soluble starch were provided from Xilong Chemical Co., Ltd, as well as manganese dioxide. The chemical compositions of red mud and fly ash were determined by X-ray fluorescence spectroscopy (XRF, Rigaku, ZSX Primus II) and the results are listed in Table 1. According to the results from XRD analysis, the crystalline phases of the two wastes are shown in Fig. 1.

Table 1 Chemical composition of fly ash and red mud (mass fraction, %)

Material	SiO_2	Al_2O_3	Na_2O	K_2O	MgO	CaO
Fly ash	54.37	24.47	1.44	1.71	0.99	4.85
Red mud	20.53	21.76	12.06	1.76	1.04	17.23

Material	Fe_2O_3	P_2O_5	MnO	TiO_2	LOI
Fly ash	5.50	0.27	0.04	1.45	4.27
Red mud	10.47	0.16	0.01	4.10	10.8

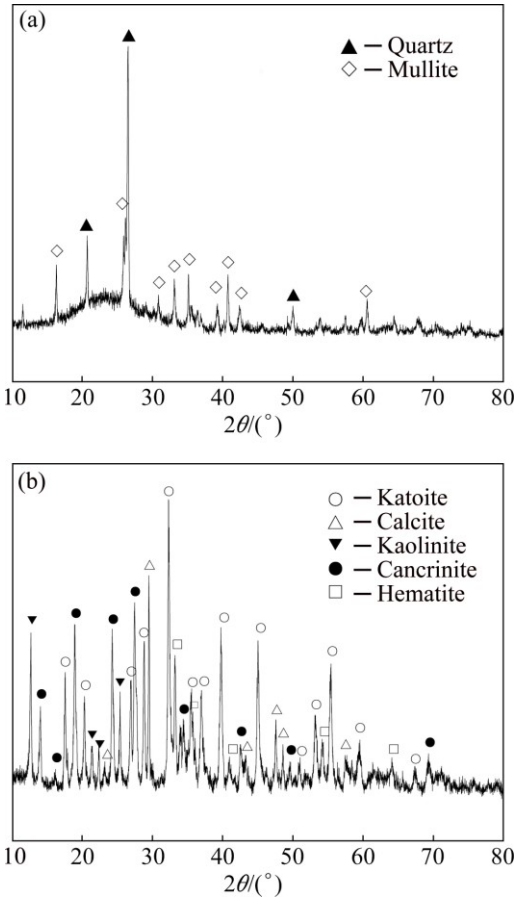

Fig. 1 XRD patterns of fly ash (a) and red mud (b)

From Table 1, both fly ash and red mud contain higher contents of SiO_2 and Al_2O_3 which are commonly used as network formers of glasses and framework compositions of ceramics. The main crystalline phases of fly ash are mullite ($Al_2O_3 \cdot SiO_2$, PDF No. 15−0776) and quartz (SiO_2, PDF No. 85−0798), while amorphous silicate glassy phase is also detected, as shown in Fig. 1(a). Compared with fly ash, the mineral phases of red mud are identified as katoite ($Ca_3Al_2(SiO_4)(OH)_8$, PDF No. 38−0368), kaolinite ($Al_2Si_2O_5(OH)_4$, PDF No. 29−1488), calcite ($CaCO_3$, PDF No. 64−9630), cancrinite ($Na_{7.6}(Al_6Si_6O_{24})(HCO_3)_{1.2}$ $(CO_3)_{0.2}(H_2O)_{2.28}$, PDF No. 70−5030), and iron oxide (Fe_2O_3, PDF No. 87−1164), as shown in Fig. 1(b). Sodium borate was added into the batches of foam ceramics as sintering aids. Starch and manganese dioxide were respectively introduced into the samples.

2.2 Sample preparation

The components of samples were mixed in a ball mill (Xianyang Jin Hong General Machinery Co., Ltd, KQM-X4Y/BC) with alumina balls (Shandong Zibo Win Chi Ceramics New Material Co., Ltd.) at speed of 180 r/min for 4 h and were sieved through 48 μm sieve after drying, and different amounts of starch (1%, 3%,

5%, 10%, 15%, mass fraction) and MnO_2 (1%, 3%, 5%, 10%, 15%, mass fraction) were added into the total composition and mixed uniformly. The samples with starch addition were named as D1, D2, D3, D4 and D5, respectively. The samples with manganese dioxide addition were named as M1, M2, M3, M4 and M5, respectively. The compositions of samples are listed in Table 2. Then, the above powder mixture about 5 g was mixed with organic binder PVA (3%) and uniaxially pressed under 5−10 MPa into the disc-shape pellets with a diameter of 25 mm and the rectangular bars with 55 mm × 6 mm × 6 mm, and then the prepared samples were dried at 100 °C for 6 h. The heating rates were 3 °C/min up to 1000 °C for 2 h in an electrical furnace with air atmosphere. A holding time of 1 h was carried at 500 °C to remove the added organic binder and inherent structural water.

Table 2 Compositions of samples (mass fraction, %)

Sample	Red mud and fly ash	Starch	MnO_2	$Na_2B_4O_7$
D1	84.0	1.0		15.0
D2	82.0	3.0		15.0
D3	80.0	5.0		15.0
D4	75.0	10.0		15.0
D5	70.0	15.0		15.0
M1	84.0		1.0	15.0
M2	82.0		3.0	15.0
M3	80.0		5.0	15.0
M4	75.0		10.0	15.0
M5	70.0		15.0	15.0

2.3 Characterization

The crystalline phases presented in the sintered samples were identified by X-ray diffraction (XRD, Rigaku D/max−2550PC). The microstructure was observed by a scanning electron microscope (SEM, FEI Quanta−200). The bulk density was obtained according to the rate of mass to volume, and the total porosity (P) was calculated from the bulk density (ρ) and powder density (ρ_0) using Eq. (1):

$$P=(1-\rho/\rho_0)\times100\% \quad (1)$$

The water absorption was measured by the waterlogged method using distilled water as liquid medium. The samples were immersed in boiling water for 5 h followed by natural cooling to room temperature. Water absorption (W) of the sample with the sizes of 5 mm × 5 mm × 5 mm was calculated from the mass of the dry samples (m_1) and soaked samples (m_2) by Eq. (2):

$$W=(m_2-m_1)/m_1\times100\% \quad (2)$$

The samples with 35 mm × 4 mm × 3 mm bars were machined for measuring the flexural strength. Square samples with 12.5 mm in length and 5 mm × 5 mm in section area were prepared and subjected to an uniaxial compressive loading. The flexural strength and compressive strength of glass ceramic foams were carried out on a CSS44100 testing machine with a cross-head speed of 1 mm/min. The support span for flexural strength test was 20 mm. Each result was obtained by calculating the average of five measurements. The acid and alkali resistances of bulk foam ceramics were measured with impregnating method according to the following formulas:

$$R_{ac}=m_{ac}/m_0 \quad (3)$$

$$R_{al}=m_{al}/m'_0 \quad (4)$$

where R_{ac} and R_{al} are the acid and alkali resistances of bulk foam ceramics, respectively; m_{ac} and m_0 are the mass of samples before and after being immersed by 0.01 mol/L hydrochloric acid, while m_{al} and m'_0 are the mass of samples before and after being immersed by 0.01mol/L sodium hydroxide solution.

3 Results and discussion

3.1 Effects of foaming agents on crystalline phases of ceramic foams

Figure 2 shows the XRD patterns of the ceramic foams with variable starch addition sintered at 1000 °C for 2 h. The phases present in the samples with starch content from 1% to 15% were different to the phases of fly ash and red mud (see Fig. 1), as well as the phases of ceramic foams using sodium silicate solution as foaming agent [25]. A typical scattered characteristic and some sharp diffraction peaks can be seen from the XRD patterns of the starch concentration of samples. This indicated that the main phases encountered in the sintered ceramics consist of amorphous glass and crystal phases. The crystal phases were sodalite phase ($Na_6(AlSiO_4)_6$, PDF No. 40−0101) [29], together with hematite (Fe_2O_3, PDF No. 87−1164), pseudobrookite

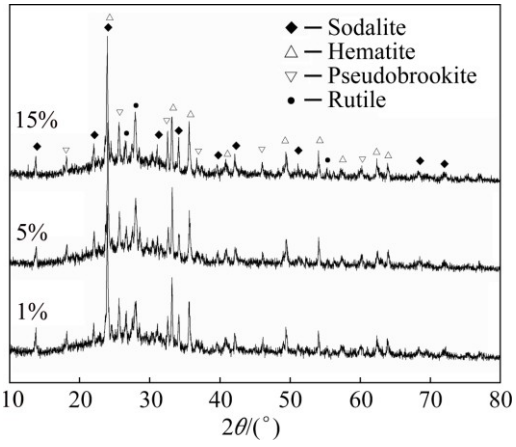

Fig. 2 XRD patterns of samples with different starch additions

(Fe_2TiO_5, PDF No. 73−1631), and rutile (TiO_2, PDF No. 88−1175). It can also be seen that the intensity and position of diffraction peaks related to four crystal phases did not appear obviously with starch contents from 1% to 15%. This indicated that all the samples had same phases and similar content of phases. On one hand, the samples with different starch additions had the similar chemical composition, as shown in Table 2. On the other hand, the added starch leaves a lot of pores in the samples during sintering process accompanied carbonization and combustion of starch, which did not cause major impact to the phases and their contents.

Figure 3 shows the XRD patterns of the samples with different MnO_2 additions sintered at 1000 °C for 2 h. Compared with the XRD patterns of the ceramic foams with starch addition, the XRD patterns of the ceramic foams with MnO_2 addition also showed typical scattered characteristic and some sharp diffraction peaks, which mean that the series of samples consist of amorphous glass and crystal phases. As the MnO_2 content increased from 1% to 15%, the four crystal phases appeared in the samples, including sodium aluminate manganese oxides $Na_8(SiAlO_4)_6MnO_4$ (PDF No. 44−1182), aluminum titanium oxide Al_2TiO_5 (PDF No. 73−1630), titanium oxide Ti_5O_9 (PDF No. 51−0641) and hematite Fe_2O_3 (PDF No. 89−0597). With the increase of MnO_2 content, more manganese ions involved in the formation of crystalline phase $Na_8(SiAlO_4)_6MnO_4$, resulting in an enhanced intensity of diffraction peaks corresponding to $Na_8(SiAlO_4)_6MnO_4$ phase. At the same time, the total content of fly ash and red mud decreased, resulting in a weaken intensity hematite due to the decrease of Fe_2O_3 in the samples. Even though the content of Al_2O_3 decreased by 2.3% for the samples from M1 to M5, the content of TiO_2 only decreased by 0.27%. As a result, the intensities of titanium oxide and titanium aluminum oxide showed a slight change.

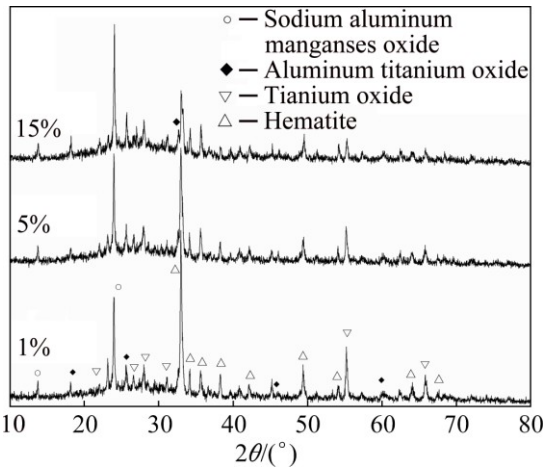

Fig. 3 XRD patterns of samples with different MnO_2 additions

3.2 Effects of foaming agents on microstructure of ceramic foams

The SEM images of the samples with starch addition sintered at 1000 °C for 2 h are shown in Fig. 4. It can be seen that the microstructure was mainly dominated by small closed pores which were caused by less amount of starch added (only 1%). The SEM image of Sample D1 appeared on uneven pore distribution and pore size due to the locally inadequate foaming area and a few of large holes from inter-connected small pores. With the fly ash content increasing to 10% (Sample D3), the size of pores increased due to the formation of inter-

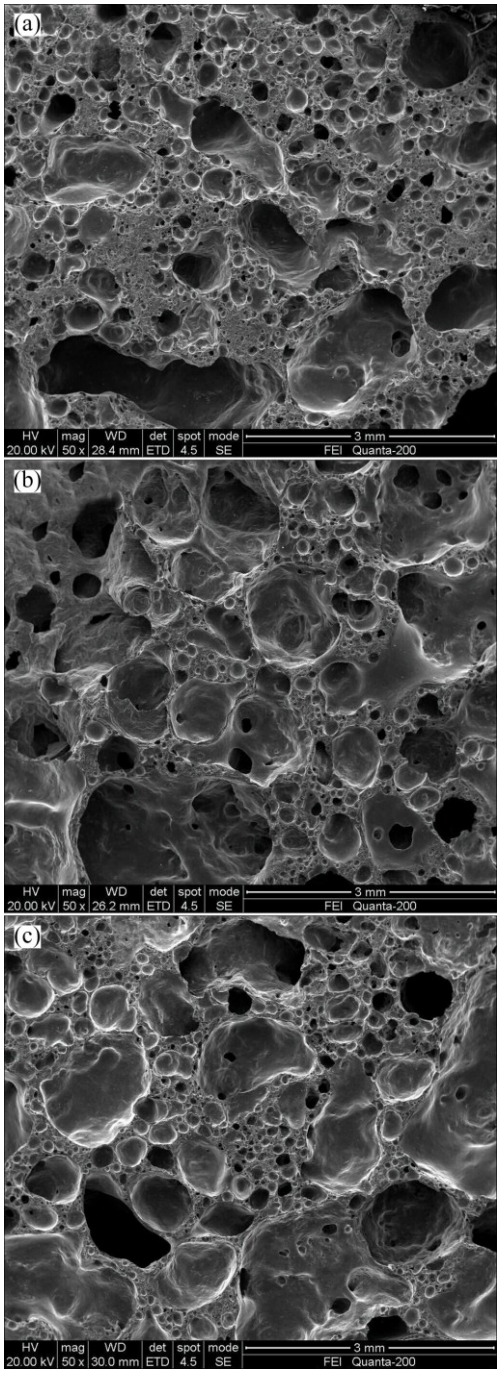

Fig. 4 SEM images of ceramic foams with different starch additions: (a) 1%; (b) 5%; (c) 15%

connection pores. In addition, the locally inadequate foaming area disappeared. Further increasing starch content into 15% (Sample D5), the locally mesh-like structure can be seen from the SEM image of Sample D5. Meanwhile, more large pores appeared in the structure of samples due to the complete foaming.

The SEM images of the samples with MnO_2 addition sintered at 1000 °C for 2 h are shown in Fig. 5. As similar to the sample with 1% starch, the microstructure was also mainly dominated by the formed small and closed pores with the size of 0.2−0.5 mm. However, an obvious difference in pore number, size and foaming area can be seen between the SEM images of Samples D1 and M1. Compared with Sample D1, Sample M1 had smaller size of pore but more locally inadequate foaming area. This indicated that the sample with 1% MnO_2 had denser structure than that of sample with 1% starch. When the MnO_2 addition increased to 10% (Sample M3), the size of pores in the samples increased with the decrease of number of closed pores because of the formation of inter-connection pores in locally areas. Further increasing MnO_2 content to 15% (Sample M5), more large pores appeared in the structure of the sample.

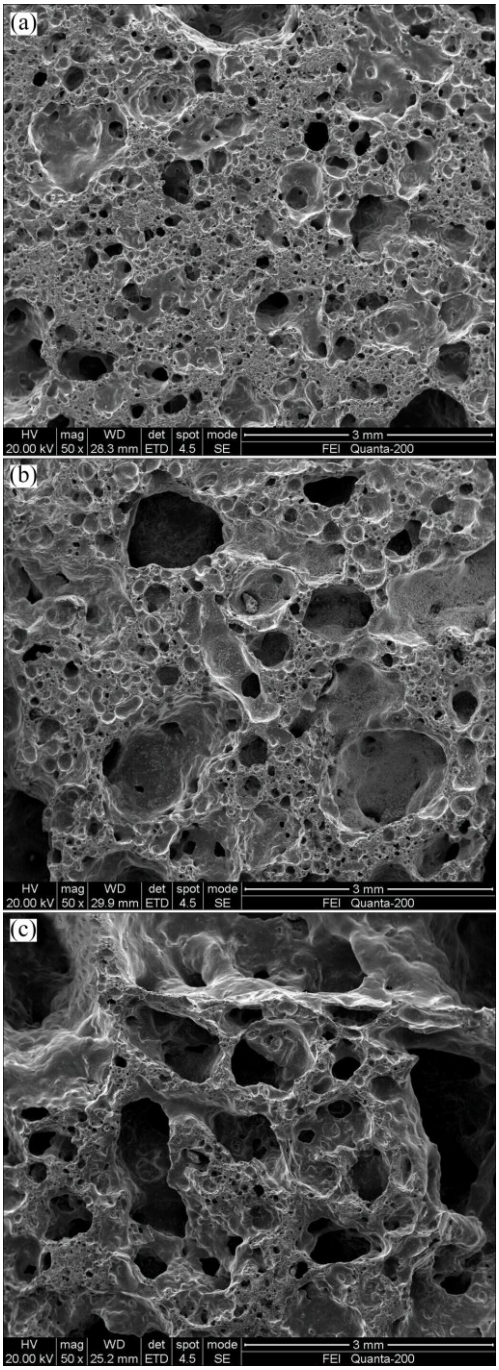

Fig. 5 SEM images of ceramic foams with different MnO_2 additions: (a) 1%; (b) 5%; (c) 15%

3.3 Effects of foaming agents on properties of ceramic foams

The relationships between foaming agent content and porosity (bulk density), porosity and properties such as mechanical strength and water absorption of the samples are shown in Figs. 6 and 7, respectively.

From Figs. 6(a) and (b), it can be seen that the porosity increased from 41.82% to 60.76% with increase of starch content from 1% to 15%. Meanwhile, the bulk density changed with an opposite tendency compared with variation of porosity. With the starch addition increasing, the bulk density decreased from 0.79 to 0.59 g/cm^3. When the sintering temperature increased, starch was carbonized and burnt with the exclusion of moisture. The residual carbon reacted with O_2 which came from air to form CO_2. The gases generated from starch reaction was wrapped by the liquid phase in sintering samples, which resulted in forming of gas cavities or cells in sintered samples. In addition, the increase of porosity of samples from D1 to D5 led to the decrease of flexural strength and compression strength, from 3.83 to 2.44 MPa and 6.04 to 4.22 MPa respectively, as shown in Fig. 6(c). It was easy to understand that the increase of the number of pores per unit volume indicated the decrease of actual bearing areas when a sample was subjected to flexural or compressive loading. Apparently, the increase of porosity was highly responsible for the declining of flexural and compression strength of the glass ceramic foams. It was also found that the water absorption of samples increased from 5.73% to 8.95% with the increase of porosity. As an important property for actual use of the porous materials, the change of water absorption should be directly related to the porosity, especially correlated with the number of opening pores in foam ceramics due to similar chemical compositions of the samples.

A similar regular variation trend of the physical–mechanical porosities of the sintered samples with MnO_2 addition is presented in Fig. 7. With the increase of MnO_2 addition from 1% to 15%, the porosity increased from 44.87% to 63.51% while the bulk

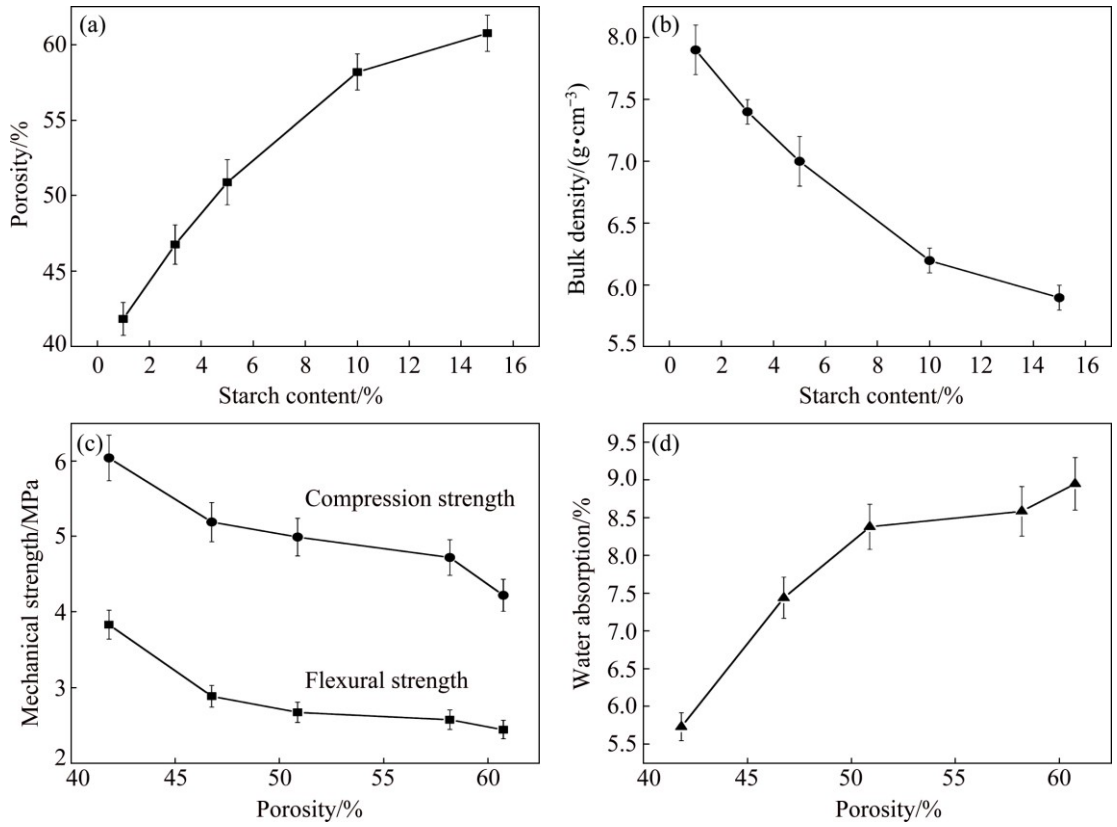

Fig. 6 Porosity (a) and bulk density (b) of samples with different starch contents, mechanical strength (c) and water absorption (d) of samples with different porosities

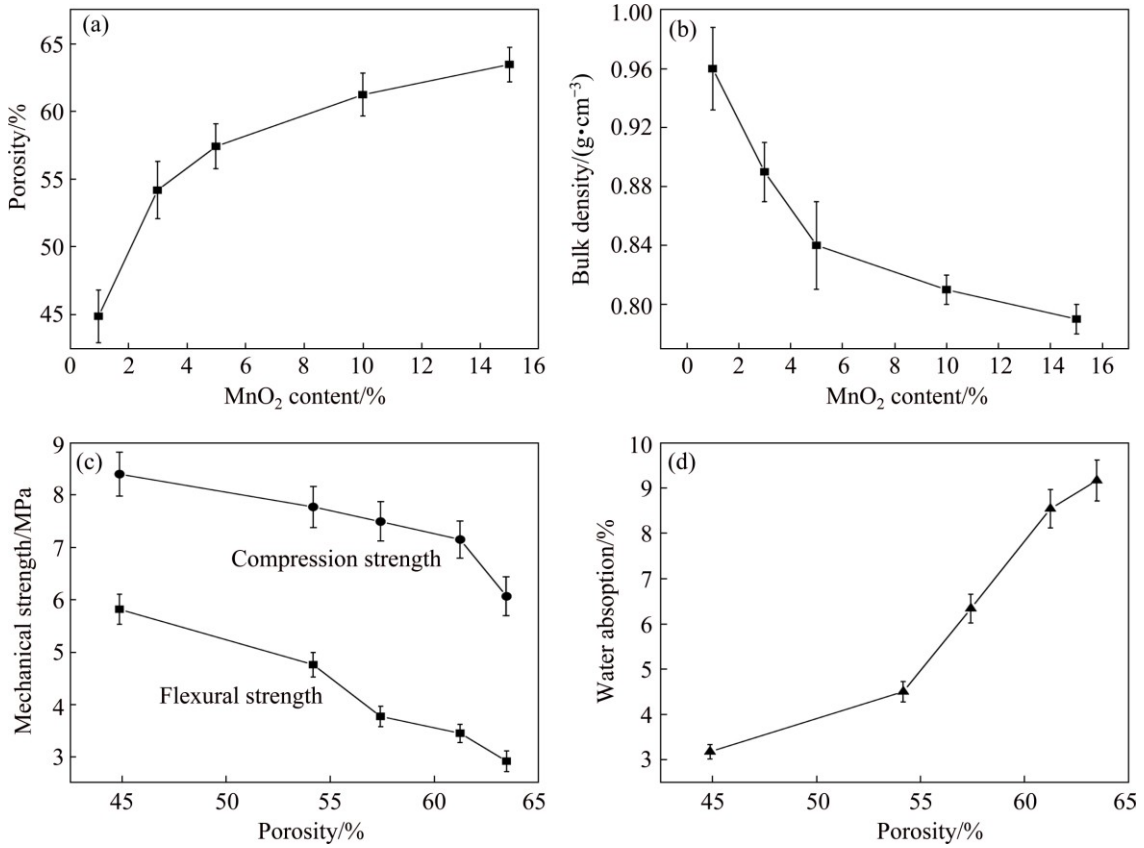

Fig. 7 Porosity (a) and bulk density (b) of samples with different MnO_2 contents, mechanical strength (c) and water absorption (d) of samples with different porosities

density decreased from 0.96 to 0.79 g/cm^3. The flexural strength and compression strength decreased from 5.82 to 2.90 MPa and 8.38 to 6.05 MPa respectively, while the water absorption increased from 3.16% to 9.17% with the increase of porosity from 41.82% to 63.51%. The minimum of bulk densities for the samples from M1 to M5 was equal to the maximum bulk density of the samples using starch as foaming agent. Moreover, the samples using MnO_2 as foaming agent had higher flexural strength and compression strength compared with the samples foamed by starch addition. This was caused by different pore structures of the samples. As shown in Figs. 4 and 5, the glass ceramic foams with MnO_2 addition had denser microstructure than the ceramic foams using starch as forming agent, which was contributed to higher mass in per unit volume and stronger capacity subjected to flexural or compressive loading of the ceramics.

Table 3 lists the acid/alkali resistances of the sintered samples using starch and MnO_2 as foaming agent, respectively. All the samples had excellent alkali resistance (higher than 99.85%) and better acid resistance (higher than 95.59%). Compared with alkali resistance, the lower acid resistance should be attributed to higher content of alkali and alkaline earth metals existing in these samples. The irregular changes between acid/alkali resistances may be caused by measuring error and not identical shape of the samples.

Table 3 Acid/alkali resistance of ceramic foams with starch or MnO_2 addition

Content	Starch addition		MnO_2 addition	
	Acid resistance/ %	Alkali resistance/ %	Acid resistance/ %	Alkali resistance/ %
1%	99.60	99.99	97.84	99.82
3%	98.97	99.85	95.59	99.93
5%	97.32	99.87	97.27	99.98
10%	98.21	99.92	97.05	99.97
15%	98.65	99.97	96.11	99.99

4 Conclusions

1) The main crystal phase in the ceramic foams with starch addition is sodalite phase ($Na_6(AlSiO_4)_6$) and the main crystal phase in the glass ceramic foams with MnO_2 addition is sodium aluminate manganese oxide ($Na_8(SiAlO_4)_6MnO_4$).

2) The SEM images show that the microstructure is mainly dominated by small closed pores and locally inadequate foaming area for two series of ceramic foams when the content of both starch and MnO_2 changes from 1% to 5%. When the content of starch or MnO_2 is higher than 5%, the porous structure of sample changes obviously, which indicates that the content of foaming agent has significant influences on porous structure.

3) There is a similar regular variation trend of properties with different foaming agent additions for the two ceramic foams. With the foaming agent addition increasing, the porosity increases while the bulk density decreases. The mechanical strength decreases while the water absorption increases with the increasing of porosity.

4) Two series of samples have excellent corrosion resistance and the ceramic foams with starch addition have better comprehensive performances (lower bulk density, higher porosity and higher strength). The results indicate that the preparation and application of red mud and fly ash based building ceramic foams may be an effective solution for the minimization of wastes and utilization of high value.

References

[1] GRÄFE M, POWER G, KLAUBER C. Bauxite residue issues: III. Alkalinity and associated chemistry [J]. Hydrometallurgy, 2011, 108: 60−79.

[2] LIU Yong, LIN Chu-xia, WU Yong-gui. Characterization of red mud derived from a combined Bayer process and bauxite calcination method [J]. Journal of Hazardous Materials, 2007, 146: 255−226.

[3] BLISSETT R S, ROWSON N A. A review of the multi-component utilisation of coal fly ash [J]. Fuel, 2012, 97: 1−23.

[4] JABEEN H, CHRISTIAN K K, CHANDRA V. Synthesis of nanozerovalent iron nanoparticles—Graphene composite for the treatment of lead contaminated water [J]. Journal of Environmental Management, 2013, 130: 429−435.

[5] NEIVA A M R, CARVALHO P C S, ANTUNES I M H R, SILVA M M V G, SANTOS A C T, CABRAL PINTO M M S, CUNHA P P. Contaminated water, stream sediments and soils close to the abandoned Pinhal do Souto uranium mine, central Portugal [J]. Journal of Geochemical Exploration, 2014, 136: 102−117.

[6] ABBASI T, ABBASI S A. Dust explosions—Cases, causes, consequences, and control (Review) [J]. Journal of Hazardous Materials, 2007, 140: 7−44.

[7] LIU Qing-ming, LI Xiao-dong, BAI Chun-hua. Deflagration to detonation transition in aluminum dust–air mixture under weak ignition condition [J]. Combustion and Flame, 2009, 156: 914−921.

[8] MILAČIČ R, ZULIANI T, ŠČANČAR J. Environmental impact of toxic elements in red mud studied by fractionation and speciation procedures [J]. Science of the Total Environment, 2012, 426: 359−365.

[9] GARAU G, SILVETTI M, DEIANA S, DEIANA P, CASTALDI P. Long-term influence of red mud on As mobility and soil physico-chemical and microbial parameters in a polluted sub-acidic soil [J]. Journal of Hazardous Materials, 2011, 185: 1241−1248.

[10] HAMER G. Solid waste treatment and disposal: effects on public health and environmental safety [J]. Biotechnology Advances, 2003, 22: 71−79.

[11] CHEN Shui-jen, HUNG Ming-cheng, HUANG Kuo-lin. HWANG Wen-lng. Emission of heavy metals from animal carcass incinerators in Taiwan [J]. Chemosphere, 2004, 55: 1197−1205.

[12] BAGHERI A, ZANGANEH H, ALIZADEH H, SHAKERINIA M, MARIAN M A S. Comparing the performance of fine fly ash and

silica fume in enhancing the properties of concretes containing fly ash [J]. Construction and Building Materials, 2013, 47: 1402−1408.
[13] SAMAL S, RAY A K, BANDOPADHYAY A. Proposal for resources, utilization and processes of red mud in India — A review [J]. International Journal of Mineral Processing, 2013, 118: 43−55.
[14] CAO Shao-tao, MA Hai-jun, ZHANG Yi, CHEN Xiao-fan, ZHANG Yi-fei, ZHANG Yi. The phase transition in Bayer red mud from China in high caustic sodium aluminate solutions [J]. Hydrometallurgy, 2013, 140: 111−119.
[15] KUMAR S, KUMAR R, BANDOPADHYAY A. Innovative methodologies for the utilization of wastes from metallurgical and allied industries (Review) [J]. Resources, Conservation and Recycling, 2006, 48: 301−314.
[16] LIU Y J, NAIDU R, MING H. Red mud as an amendment for pollutants in solid and liquid phase [J]. Geoderma, 2011, 163: 1−12.
[17] WANG S B, ANG H M, TADÉ M O. Novel applications of red mud as coagulant, adsorbent and catalyst for environmentally benign processes [J]. Chemosphere, 2008, 72: 1621−1635.
[18] PULFORD I D, HARGREAVES J S J, ĎURIŠOVÁ J, KRAMULOVA B, GIRARD C, BALAKRISHNAN M. Carbonised red mud-a new water treatment product made from a waste material [J]. Journal of Environmental Management, 2012, 100: 59−64.
[19] AGATZINI-LEONARDOU S, OUSTADAKIS P, TSAKIRIDIS P E, MARKOPOULOS C. Titanium leaching from red mud by diluted sulfuric acid at atmospheric pressure [J]. Journal of Hazardous Materials, 2008, 157: 579−586.
[20] AMRITPHALE S S, ANSHUL A, CHANDRA N, RAMAKRISHNAN N. A novel process for making radiopaque materials using bauxite–red mud [J]. Journal of the European Ceramic Society, 2007, 27: 1945−1951.
[21] YANG Jia-kuan, ZHANG Du-du, HOU Jian, HE Bao-ping, XIAO Bo. Preparation of glass-ceramics from red mud in the aluminium industries [J]. Ceramics International, 2008, 34: 125−130.
[22] VINCEZNO M S, STEFANO M, ALEXIA C, ANTONIO S, GIOVANNI C, GIORGIO C. Bauxite ‘red mud’ in the ceramic industry. Part 2: Production of clay-based ceramics [J]. Journal of the European Ceramic Society, 2000, 20: 245−252.
[23] CHEN Bo, LUO Zhi-wei, LU An-xian. Preparation of sintered foam glass with high fly ash content [J]. Materials Letters, 2011, 65: 3555−3558.
[24] CHEN Bo, WANG Ke-qiang, CHEN Xing-jun, LU An-xian. Study of foam glass with high content of fly ash using calcium carbonate as foaming agent [J]. Materials Letters, 2012, 79: 263−265.
[25] CHEN Xing-jun, LU An-xian, QU Gao. Preparation and characterization of foam ceramics from red mud and fly ash using sodium silicate as foaming agent [J]. Ceramics International, 2013, 39: 1923−1929.
[26] ZIVCOVÁ Z, GREGOROVÁ E, PABST W, SMITH D S, MICHOT A, POULIER C. Thermal conductivity of porous alumina ceramics prepared using starch as a pore-forming agent [J]. Journal of the European Ceramic Society, 2009, 29: 347−353.
[27] PETERSEN R R, KÖNIG J, YUE Y Z. The mechanism of foaming and thermal conductivity of glasses foamed with MnO_2 [J]. Journal of Non-Crystalline Solids, 2015, 425: 74−82.
[28] KÖNIG J, PETERSEN R R, YUE Yuan-zheng. Fabrication of highly insulating foam glass made from CRT panel glass [J]. Ceramics International, 2015, 41: 9793−9800.
[29] GUO Yu-xi, ZHANG Yi-he, HUANG Hong-wei, MENG Ke, HU Kun-ran, HU Pan, WANG Xin-ke, ZHANG Zhi-lei, MENG Xiang-hai. Novel glass ceramic foams materials based on red mud [J]. Ceramics International, 2014, 40: 6677−6683.

以淀粉和二氧化锰为发泡剂的赤泥–粉煤灰基泡沫陶瓷

侯丽君，刘涛涌，卢安贤

中南大学 材料科学与工程学院，长沙 410083

摘　要：分别以淀粉和二氧化锰分别为发泡剂，以硼酸钠为助溶剂，成功制备以赤泥和粉煤灰为主要原料的泡沫陶瓷。研究了淀粉或二氧化锰的含量对泡沫陶瓷中物相、孔形态及理化性能的影响。结果表明，以淀粉或二氧化锰为发泡剂制备的泡沫陶瓷的主晶相分别为 $Na_6(AlSiO_4)_6$ 和 $Na_8(SiAlO_4)_6MnO_4$；扫描电镜观察结果表明，发泡剂含量对泡沫陶瓷中气孔结构的形成起决定性作用；随着发泡剂含量的增加，泡沫陶瓷表现出优良的综合性能：体密度 0.59~0.96 g/cm^3，气孔率 41.82%~63.51%，吸水率 3.16%~9.17%，抗压强度 4.22~8.38 MPa，抗弯强度 2.44~5.82 MPa，耐酸性 95.59%~99.60%和耐碱性 99.82%~99.99%。所制备的泡沫陶瓷适合用作建筑物的隔热、保温、隔声与防火材料。

关键词：赤泥；粉煤灰；淀粉；二氧化锰；泡沫陶瓷

(Edited by Xiang-qun LI)